



Tidal and Residual Circulation in the Gulf of Khambhat and its Surrounding on the West Coast of India

R. K. Nayak · M. Salim · D. Mitra · P. N. Sridhar ·
P. C. Mohanty · V. K. Dadhwal

Received: 25 November 2013 / Accepted: 27 April 2014 / Published online: 12 July 2014
© Indian Society of Remote Sensing 2014

Abstract A terrain-following ocean model is implemented for simulating three-dimensional tidal and residual circulations in the Gulf of Khambhat and its adjacent oceans on the west coast of India. The model is forced with time varying tidal levels and momentum fluxes at the western and southern boundaries. Simulated tidal levels and currents compare well with the observation at tide gauge and current-meter stations. Estimated residual circulation in the region has several notable features that include strong southward along channel flow inside the gulf, northwestward propagating coastal boundary jet currents parallel the 60 m isobaths, southward slope currents, alongshore coastal currents on the southeastern flank of the shelf and a number of meso-scale eddies. All these features of residual circulation are captured well by the satellite imagery of Chlorophyll concentration mapped in the month of March, the period when tide plays dominant role on the control of net circulation in the region.

Keywords Tide · Residual circulation · Continental shelf circulation · Coastal circulation · Tides · Coastally trapped waves · West coast of Indian

Introduction

Western continental shelf of India varied from south to north and widest off Bombay, leads into strongly converging channel, the Gulf of Khambhat (GK). This region is of immense interest among researchers considering various ongoing industrial activities (navigational, oil and gas industry etc.) and proposed developmental projects like impounding fresh water, harnessing tidal and thermal energy etc. The GK and its surrounding (Fig. 1) can be broadly divided into inner-outer gulf, continental shelf and continental slope. The gulf extends from upstream to a depth of 30 m with 120 km long and 50 km wide mouth. The continental shelf spans 200–250 km from gulf mouth to 200 m depth contour. The continental slope spans beyond 200 m depth contour extends to the abyssal depth. The inner gulf is gentle curving with irregular surface topography, whereas the outer gulf is straight sloping gentle topography (with funnelling shape). The gulf head is reworked by Mahi sagar river channel and meandering with formation of sand bank (MAL Bank) on left bank of the gulf. GK experiences largest tidal range along the Indian coast. Tides in this region are of mixed semi-diurnal undergoing strong amplification in the gulf. Study of tidal circulation in this region is of great interest to many researchers. Unnikrishnan et al. (1999) developed a barotropic numerical hydrodynamic model for simulation of observed feature of tidal amplification in the gulf. Nayak and Shetye (2003) used the one-dimensional version of the barotropic model to examine the causes of tidal amplification in GK and they concluded that resonance together with geometrical effects and friction setup the amplification of semi-diurnal tides in the Gulf.

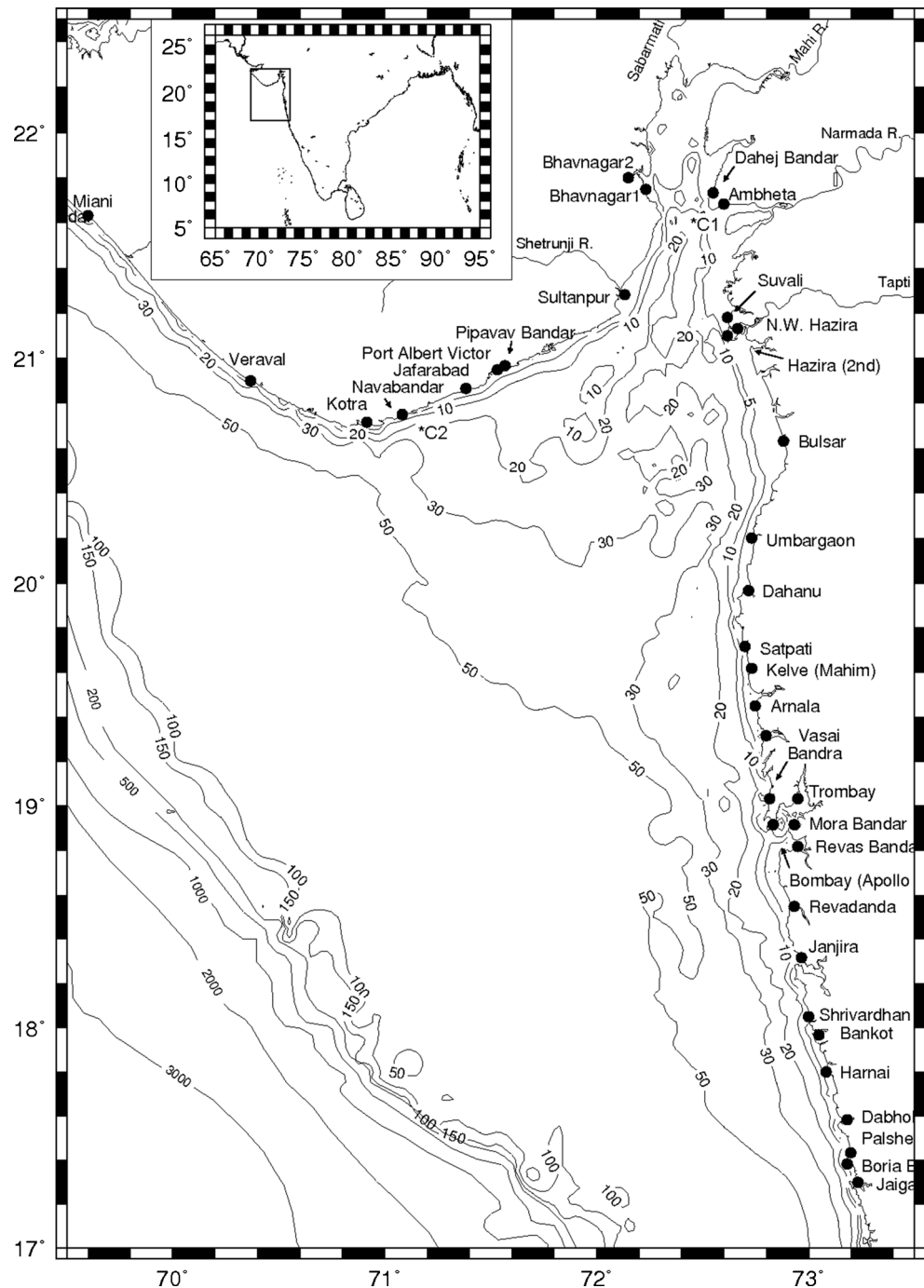
R. K. Nayak (✉) · M. Salim · P. N. Sridhar · V. K. Dadhwal
Earth and Climate Science Area, National Remote Sensing Centre
(NRSC), ISRO, Balanagar, Hyderabad, India 500625
e-mail: rabin2005@rediffmail.com

D. Mitra
Indian Institute of Remote Sensing (ISRO), Kalidas Road, Dehradun,
India 403004

P. C. Mohanty
Indian National Centre for Ocean Information Services (INCOIS),
Hyderabad, India

M. Salim
Center for Earth Atmosphere and Weather Modification
Technologies (CEA & WMT), Jawaharlal Nehru Technological
University (JNTU), Hyderabad, India 500 085

Fig. 1 Study region with depth contours and location of tidal stations (solid black dots) and two current meter measurement stations (C1 and C2)



Tidal strength is an important agent in driving and modulating net circulation in a semi-enclosed water body. Occurrence of barotropic slope currents following isobaths are common features of shelf seas in non-equatorial regions (Li and McClimans 2000). Tidal flow over the topographical features such as sill and continental shelf slope in a stratified ocean can produce internal waves of tidal frequency (Rattray et al. 1969; Hibiya 2004). Asymmetries in the flood and ebb tide due to bottom friction and non-uniform bathymetry can induce

residual flow (Robinson 1981; Geyer and Signell 1990). Several observational studies reported the evidence of intensified residual currents flowing parallel to the continental slope as well as enhanced baroclinic tidal motion and fluctuations corresponding to internal gravity waves and longer period slope waves (Huthnance 1986; Thorpe 1992). The theory of existence of barotropic slope currents under the influence of strong tidal forcing, the process of tidal rectification, was examined by Garreau and Mazé (1992) and Mazé et al. (1998).

We believe that the GK and its adjacent oceans with its complex topography and geometry could manifest complex 3D circulation driven by tides and other external forcing. This circulation pattern has strong influence on the control of various tracer transport and biogeo chemistry occurring in this coastal environment. Thus, there is need of establishment of a 3D circulation model in this region. In view of this, the present study aims to set up a 3D numerical ocean model to understand tidal and residual circulations in the GK and its adjacent oceans. This study further extends the scope for addressing other aspect of coastal circulation in this region.

Methodology

In the present study, we used the Princeton Ocean Model (POM) developed by Blumberg and Mellor (1987). The POM is a terrain following three dimensional ocean circulation model most suited for coastal ocean processes studies. It has been used in several cases for modeling internal tides and residual currents in coastal waters (Holloway 1996; Robertson 2001). The model solves finite difference analogs of the primitive equations, with a non-linear equation of state relating density to the temperature and salinity. Vertical mixing coefficients for momentum and tracers are parameterized based on 2.5 turbulent kinetic energy closer schemes of Mellor and Yamada (1982), whereas horizontal mixing coefficients are modeled with Smogorinsky formulation for diffusion. Bottom frictional stresses are modeled based on logarithmic law of the wall modified for the coastal region for which bottom boundary layer is not well resolved according to Denniss and Middleton (1994). The model employs a C grid in the horizontal and a terrain following sigma coordinate for the vertical. The horizontal time differencing is explicit whereas the vertical differencing is implicit. The model has a free surface and a split time step: the external mode portion of the model is two-dimensional and uses a short time step based on the Courant-Friedrichs-Levy (CFL) condition and the external wave speed, whereas the internal mode is three-dimensional and uses a long time step based on the CFL condition and the internal wave speed. In the present case, model grid of the study region (69.5–72.3°E and 17–22.2 °N) consists of uniform Cartesian coordinate system at 5 km (~2 min) resolution (121 levels along longitude, 163 level along the latitude) for the horizontal and 24 sigma-layers for the vertical. The bathymetric data used for this purpose are from corrected ETOPO-2 for the Indian coast (www.nio.org). LANDSAT map was used to correct geometry of the gulf, especially around the upstream end of the gulf. Time steps for the external barotropic and internal baroclinic modes are taken as 6 s and 1 min respectively. Temperature and Salinity data to describe initial stratification for the model ocean are taken from the Levitus (1982) climatological

database. Temperature and salinity data are extrapolated (by simply using the nearest neighbour valid pixel) to fill the data gaps on the near shore region including the upstream end of the Gulf. The model run is carried out for 62 days by forcing with time varying tidal level and feeble currents at western and southern boundary. Excluding the first 3 days run, remaining 59 days model output were used for the analysis in the paper. It is worth mentioning here that these three days spin up period is enough for the model to reach a stable state as the region is very small and dominated by M2 tides (also inferred from the kinetic energy analysis).

Data of amplitude and phases of five major tidal constituents (M2, S2, N2, O1, and K1) to specify tidal level at the western and southern boundaries are based on global tidal model FES99 (Lefèvre et al. 2002). The feeble currents to specify momentum fluxes at western and southern boundaries were representative of spring season (March and April) and were based on Simple Ocean Data Assimilation climatology (Carton and Giese 2008). This period is selected for the model run for the following reasons. 1) This is the period when wind over this region is weak and tides suppose to have significant control on the net circulation patterns inside the embayment. 2) The study domain is subjected to very small lateral momentum fluxes at the western boundary (+1 Sv = $10^6 \text{ m}^3 \text{ s}^{-1}$) and out flux (−1 Sv) at the southern boundary. 3) In this period, the sky is mostly cloud free and satellite picture of chlorophyll c2concentration is available to infer/validate residual currents in the study domain.

Residual circulation is the mean circulation that can be estimated from simulated currents in GK using following procedure. As shown in Eq. 1, the instantaneous current (U) is composed of steady residual flow (U_0), tidal-harmonics component (the second term) and perturbation term (U_ϵ). Tidal harmonics were estimated from the simulated currents using least square procedure (Foreman 1978). Then the differences between simulated currents and tidal harmonics were averaged over several days (here entire duration of simulation period excluding first two days) to compute the steady residual circulation.

$$U = U_0 + \sum U_{ai} \text{Cos}(\omega_i t + \psi_i) + U_\epsilon \quad (1)$$

Results

Comparison with in Situ Observations and Global Tidal Solutions

Historical tidal observations in the form of amplitude and phases of major tidal constituents at 37 coastal stations across the study region (see Fig. 1) are used for examining the performance of the model results. The observations are taken

from special publication by International Hydrographic Bureau (1930), and subsequent publications; and volume 2 of Admiralty tide tables (1996). Spectral analysis of the simulated sea levels at respective coastal stations based on least square procedure (Foreman 1978) is carried out to estimate amplitudes and phases of the major tidal constituents. Comparison between simulated results and the observations is presented in the form of scatter plots (Fig. 2a–b). Root mean square errors (rmse) between predicted and observed tidal levels (due to each tidal component) at all tide gauge stations are calculated based on following expression and are presented in Table 1.

$$rmse = \sqrt{\frac{1}{L} \sum_i (A_m \cos(\omega_i t - \psi_m) - A_o \cos(\omega_i t - \psi_o))^2} \quad (2)$$

Where L is the total temporal segments; A_m (Ψ_m) and A_o (Ψ_o) are amplitudes (phases) of modelled and observed tides respectively. The index i range between 1 and L .

There exists good agreement between observations and the simulation for both amplitudes and phases of major diurnal (K1, O1) and semi-diurnal (S2, M2) tidal constituents. Alike the observations, the predicted sea levels in the gulf is dominated by semi-diurnal tides and exhibit large change in phases. Amplitudes of diurnal tides are relatively small and associated with small change in phase. However, there are three stations, namely Bhavanagar, Dahej and Suvali, where model estimated M2 and S2 amplitudes are much smaller than the observations. These stations are located in the tidal flat region in the inner gulf. As the tidal flat regions are poorly represented in the model, large errors are estimated in these stations.

The FES99 and FES04 are global tidal solutions (Lefèvre et al. 2002; Lyard et al. 2006), respectively with 0.25° and 5 min spatial resolution and are available at the public domain along with TOPEX/Poseidon Sea Surface height (SSH) observations. These tidal solutions are used for different oceanographic applications: tidal correction for satellite measured SSH data for the analysis of sea level change controlled by processes other than the tide; used as forcing in the coastal circulation model to simulate circulation pattern in a tide dominated embayment such as the GK and its surrounding, etc. The validity of FES tidal solutions in GK were also examined in Fig. 2a and b. Prior to this, we applied following correction for the phase angles of FES tide in order to convert them from the reference of Greenwich Mean Time (GMT) to standard local time zone.

$$g_i = G_i - \frac{360^\circ}{P_i} Z_n \quad (3)$$

Where g_i and G_i are phase angles of the tidal constituent, i , with reference to the local time and GMT respectively. P_i is the period of the tide (in hours) and Z_n is the time zone of the

Fig. 2 a The scatter plots show the comparison between amplitudes of observed and predicted tides at 37 coastal tide gauge stations around GK. Different symbols: O is for present modelling results (POM), X is for FES99 and + is for FES99. **b** Same as the (a), but for the phases of major tides instead of amplitudes

location. The present study region belongs to zone number 5. Thus, 75° and 150° corrections required for diurnal and semi-diurnal tides, respectively.

The comparison of FES99 tides with observations suggests that FES tidal amplitudes are comparable with the observations however, small values are over estimated and large values are under estimated. FES99 tidal phases are also comparable with observations. The rmse associated with FES99 tidal levels (Table 1) are significantly larger at the stations located across the gulf regimes and are small for the stations located on the outer domain of the embayment. Errors associated with FES04 are larger than the errors with FES99.

The simulated ocean currents are compared with available observations: Aanderaa Doppler current meter measurement at 72.5°E, 21.66°N (Kumar and Kumar 2010) and moored buoy observation at 71.49°E, 20.8°N deployed by National Institute of Ocean Technology, Chennai (Data sources INCOIS webpage). The former observation is located in the inner gulf regime (*C1 in Fig. 1) and later is located in the northern part of the gulf mouth (*C2 in Fig. 1). Table 2 shows comparison between model and observed currents in the form of amplitude and phases of major tidal harmonics. It revealed that simulated currents compare well with the observations. At the inner gulf, both simulated and model currents are mostly alongshore, dominated by M2 tide with observed amplitude of 165 cm s⁻¹ and 262° phase, while it was 153 cm s⁻¹ and 252° in simulated results. At the station *C2 (gulf-mouth), both model and observation are comparable and have equal magnitude of alongshore and cross-shore components. In this station currents are primarily dominated by M2 tide followed by S2 and N2 tides (see Table 3). The current at this location is weaker than that of the inner gulf station.

Spatial Pattern of Amplitude and Phases of Major Tides

The spatial pattern of amplitude and phase of major tidal constituents (M2, S2, K1 and O1) are presented in Fig. 3. M2 co-tidal lines (contour of equal phase) are aligned across the axis of the channel suggesting the tidal propagation is along the channel, northeast and southwest direction. It has undergone continuous change by 225° from far-slope regime towards the inner gulf: 325° at the shelf break; 360° at the mouth of the gulf and 105° at the inner gulf. M2 co-range lines (contour of equal amplitudes) parallel the eastern coastal boundary indicating dominance of coastal Kelvin waves on M2 tidal propagation

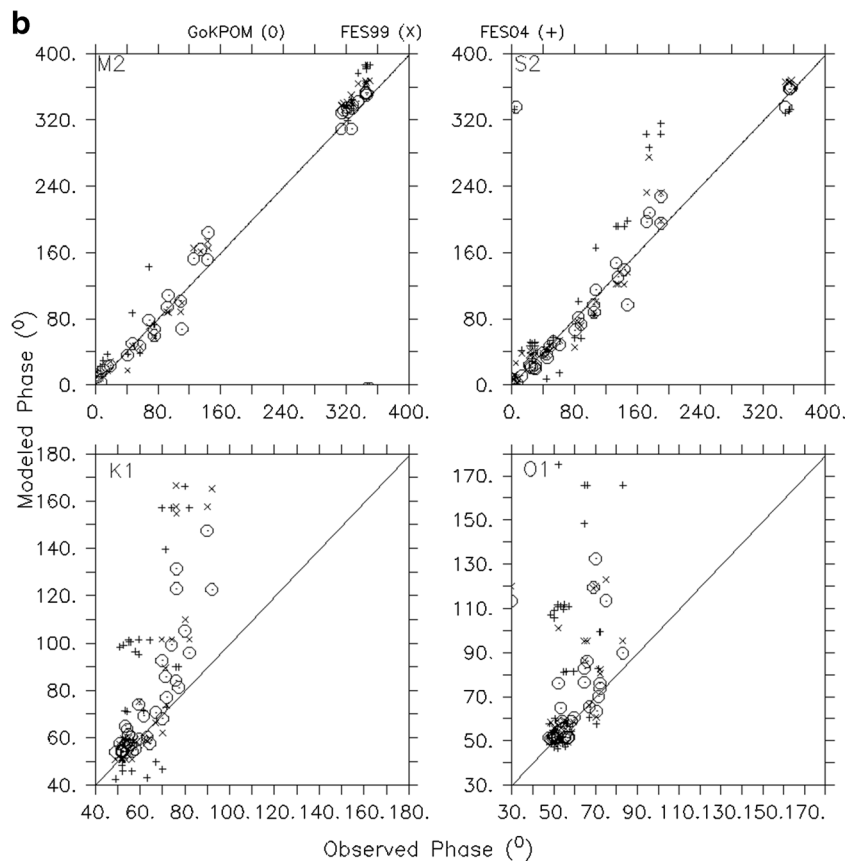
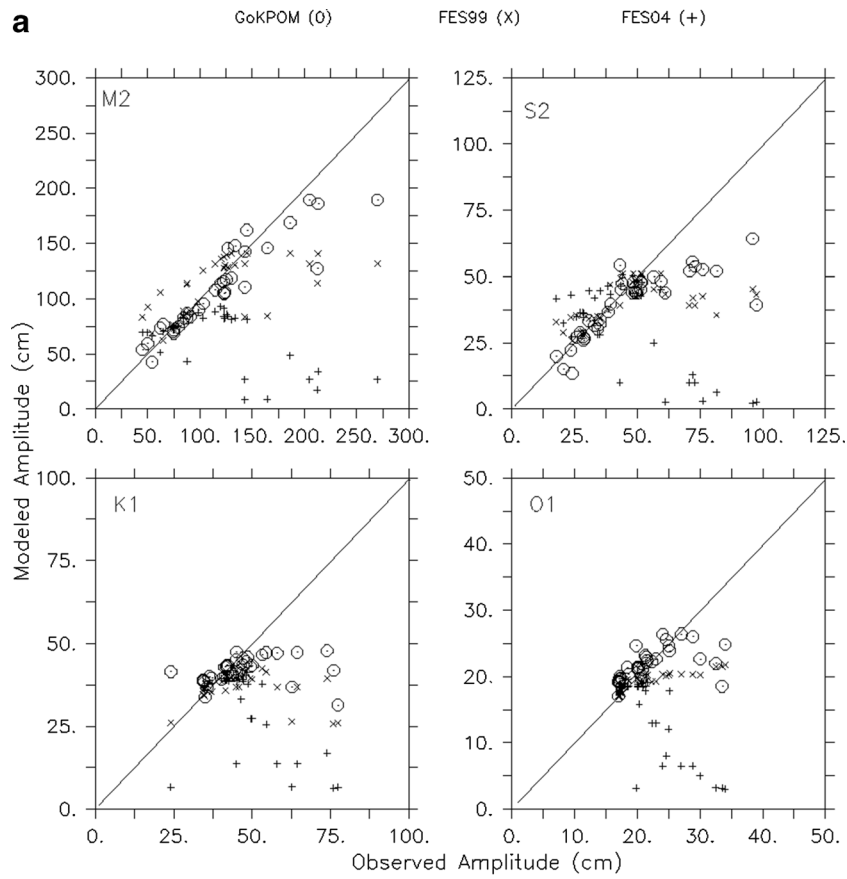


Table 1 Comparison of observed tidal harmonics at coastal tide gauge stations and our model results. “A” represents amplitude (in cm) and “G” represents phase (in degree) of tidal harmonics; associated indices: “o” is for observed and “m” is for model; R is the root mean square error of predicted tidal levels

Name of stations	M2					S2					K1					O1				
	Ao	Go	Am	Gm	R	Ao	Go	Am	Gm	R	Ao	Go	Am	Gm	R	Ao	Go	Am	Gm	R
Porbandar	65	314	77	309	8	24	349	13	336	7	35	56	34	60	1	17	54	17	59	0
Vereva	54	327	43	309	8	21	5	15	336	4	36	63	37	60	1	18	59	19	59	1
Kotra	45	0	54	12	6	18	44	20	37	2	40	70	39	68	1	21	70	20	63	1
Nawabandar	50	19	59	24	7	24	61	22	49	1	44	67	40	71	3	21	67	20	65	0
Jafarabad	62	57	73	47	8	26	88	27	73	1	47	72	42	77	3	20	71	21	70	1
Albert	87	75	82	60	4	34	105	30	88	3	50	77	43	81	5	22	72	22	74	0
Piva	88	75	87	68	1	35	104	32	97	2	50	76	43	84	5	23	72	23	76	0
Sul_cambay	212	110	127	68	51	82	147	52	97	17	999	80	60	105		30	52	23	76	5
Bhavnagar1	314	143	172	152	88	96	190	64	195	18	76	92	57	123	14	34	75	25	114	6
Bhavnagar2	143	144	111	184	15	98	190	39	228	38	77	90	46	147	22	34	70	19	132	11
Dehej	312	125	173	153	86	61	172	44	197	9	24	76	41	123	12	20	30	25	113	3
Ambheta	165	134	146	164	5	76	175	53	208	13	63	76	52	131	8	33	69	22	119	7
Suvali	270	93	189	108	44	73	133	54	147	10	58	74	62	99	3	24	83	26	90	2
N.w.hazira	205	109	189	102	11	43	143	54	140	8	45	82	47	96	2	27	66	26	86	0
Hazira2	143	92	143	94	0	71	135	52	130	13	64	70	62	93	1	29	65	26	83	2
Bulsar	213	68	186	79	19	72	107	56	115	12	74	71	63	86	8	25	65	26	77	1
Umbargaon	186	47	169	50	12	57	85	50	82	5	55	59	62	74	5	25	53	25	65	0
Dahanu	145	41	162	36	12	59	80	48	66	8	53	62	47	69	5	25	60	24	61	1
Satpati	130	16	119	23	8	51	53	48	52	2	49	53	46	65	2	21	56	23	57	1
Kelve	126	10	117	18	6	52	49	48	47	3	47	54	46	64	1	21	55	23	56	1
Amala	123	2	116	10	5	48	40	48	39	0	45	55	45	61	0	22	54	22	54	1
Vasai	120	6	114	4	4	44	45	47	33	2	48	60	44	59	3	21	50	22	53	1
Bandra	115	346	108	-5	9	43	23	45	24	1	42	51	44	58	1	20	50	21	51	1
Apol	123	345	105	352	13	48	25	44	21	3	42	55	43	57	1	20	52	21	51	1
Prince	124	345	106	353	13	49	23	44	22	3	43	55	43	57	1	20	52	21	51	1
Trombay	134	350	148	-5	14	51	30	45	24	4	47	64	44	58	3	18	55	21	51	2
Uran	127	347	145	352	13	50	29	44	21	4	42	56	43	57	1	20	57	21	51	1
Revas	123	346	105	350	13	50	29	44	19	4	41	53	43	57	1	21	55	21	51	0
Revadanda	103	335	96	342	5	39	13	40	11	0	45	58	42	55	2	19	49	20	51	1
Janjiri	99	327	90	338	6	38	3	37	7	1	46	52	41	55	3	17	51	20	51	2
Shrivaedha	91	322	84	335	5	35	0	34	4	1	42	52	40	54	1	17	48	20	51	2
Bankot	85	328	83	334	1	31	6	33	2	2	36	56	40	54	3	17	57	20	51	2
Harnai	84	317	79	332	3	33	356	31	360	1	37	49	40	54	2	18	50	20	52	1
Dabhol	79	322	74	330	3	27	3	29	-1	1	35	54	39	54	3	17	56	19	52	2
Palshet	75	314	71	329	2	28	355	27	358	1	34	52	39	54	3	17	50	19	52	1
Boria	75	314	70	329	3	29	354	27	358	1	34	52	39	54	3	17	50	19	52	2
Jaigarh	75	315	69	329	4	29	354	26	358	2	35	52	38	54	3	17	52	19	52	1

in the region. Amplitude of M2 tide was 40 cm at the far-slope region, and undergoes slow amplification over the continental slope untills the shelf break. On the continental shelf, it has undergone strong amplification, more than 3 times (40 to 150 cm) towards the inner Gulf. It remains uniform inside the inner gulf and decrease further towards gulf head (up to 70 cm). Strong amplification of

semidiurnal tides in the continental shelf and in main gulf (except gulf head regions) is an important characteristic of this embayment resulted from the quarter wavelength resonance of the tides owing to its inherent geometrical settings (Nayak and Shetye 2003).

Spatial pattern of S2 tidal chart is similar to M2 tide; however, S2 amplitude is almost half of M2. On the other

Table 2 Root mean square errors (R) in the present model (GK-POM) solution and its comparison with global FES tidal solutions at 37 tide gauge stations

Name of stations	Total R for POM (cm)	Total R for FES99 (cm)	Total R for FES04 (cm)
Porbandar	16	14	17
Vereva	14	19	19
Kotra	9	41	37
Nawabandar	10	42	32
Jafarabad	13	43	27
Albert	11	29	58
Piva	8	30	60
Sul_cambay	74	108	172
Bhavnagar1	126	244	355
Bhavnagar2	86	125	234
Dehej	111	178	281
Ambheta	33	114	222
Suvali	58	139	260
N.w.hazira	21	65	186
Hazira2	17	56	177
Bulsar	39	100	221
Umbargaon	23	53	150
Dahanu	25	28	71
Satpati	14	15	49
Kelve	11	17	39
Amala	6	17	29
Vasai	10	23	31
Bandra	12	19	24
Apol	17	12	34
Prince	18	10	38
Trombay	23	13	48
Uran	19	8	37
Revas	19	9	38
Revadanda	9	26	23
Janjiri	13	10	19
Shrivaedha	9	7	14
Bankot	7	7	13
Harnai	8	4	14
Dabhol	10	4	12
Palshet	8	3	13
Boria	9	2	12
Jaigarh	10	4	11

hand, diurnal tides (K1, and O1) have small amplitudes, 35 cm and 18 cm at the shelf break respectively for K1 and O1 tides, and they exhibit slow amplification towards the inner gulf. At the gulf head, amplitudes are 65 cm and 30 cm respectively. Unlike the semidiurnal tides, phases of diurnal tides exhibit small change (25°–50° for K1 and 35°–80° for O1) from the shelf break towards the inner gulf. Orientation of the co-tidal lines suggests that semi-diurnal tides propagate along south- north direction.

Depth Average Currents and Surface Currents

The typical flood and ebb phases of tidal levels and currents in the study domain as shown in Fig. 4 suggest that the flood phase sea level is high (~75 cm) at the far-slope region, decreases gradually towards the shelf break and became neutral at the gulf mouth (Fig. 4a). It decreases further down to –200 cm in the inner gulf. Head of the gulf manifest a positive sea level isolates from inner gulf and open oceans. Simulated

Table 3 Comparison of simulated currents with observations at two stations: Aanderra Doppler Current Meter measurement station C1 (72.5°E, 21.66°N) (Kumar and Kumar 2010) and at the moored buoy

observation station C2 (71.49°E, 20.8°N) (see Fig. 1. U is zonal currents and V is meridional currents. Indices “a” and “b” represent amplitude (in cm s^{-1}) and phase (in degree) of harmonics

	Tidal harmonics	Observed currents				Modeled currents			
		Ua	Up	Va	Vp	Ua	Up	Va	Vp
At Aanderra Doppler Current meter station	M2	11	45	165	262	13	273	153	252
	S2	3	300	49	312	8	108	48	183
	K1	6	135	24	295	2	107	32	165
	O1	4	260	6	267	1	230	16	237
	N2	1	259	40	244	5	194	43	290
At moored buoy station	M2	42	25	59	4	79	145	43	144
	S2	29	46	28	47	30	75	16	73
	K1	11	358	13	22	18	154	9	141
	O1	14	38	20	42	9	196	5	196
	N2	26	337	27	330	21	190	11	187

vertical average currents (barotropic currents) mostly flow across the tidal level on the continental shelf and gulf regimes. They are weak on the continental slope regime (less than 10 cm s^{-1}) and are intensified over the shelf regime (50 cm s^{-1}) and proceeds into the gulf where they further intensified up to 150 cm s^{-1} at the gulf head. During the ebb phase, the sea level increases from negative values (-75 cm) over the slope regime towards the shelf with zero tidal level at the gulf mouth (Fig. 4b). Tidal level further increased up to maximum 200 cm towards the inner gulf and then decreased down to 50 cm at the gulf head. During this time, barotropic currents exhibit westward flow (from GK to open ocean) on the continental shelf. The currents are strong (100 cm s^{-1}) inside the Gulf and their magnitude decreases towards the slope break (10 cm s^{-1}). Surface current features almost resemble the features of the barotropic currents (Fig. 4c–d) over the continental shelf and gulf regions. However, they are stronger than the barotropic currents over the open ocean regime, beyond the shelf break. These are associated with anti-cyclonic and cyclonic eddy features during flood and ebb phases respectively. These circulation features and associated eddies usually occur in deep water beyond the shelf break owing to the consequence of instability of baroclinic currents associated with anomalous velocity shear with respect to surrounding water masses against the steep bathymetry on the continental slope (Barltrop 1998).

Vertical Structure of Currents

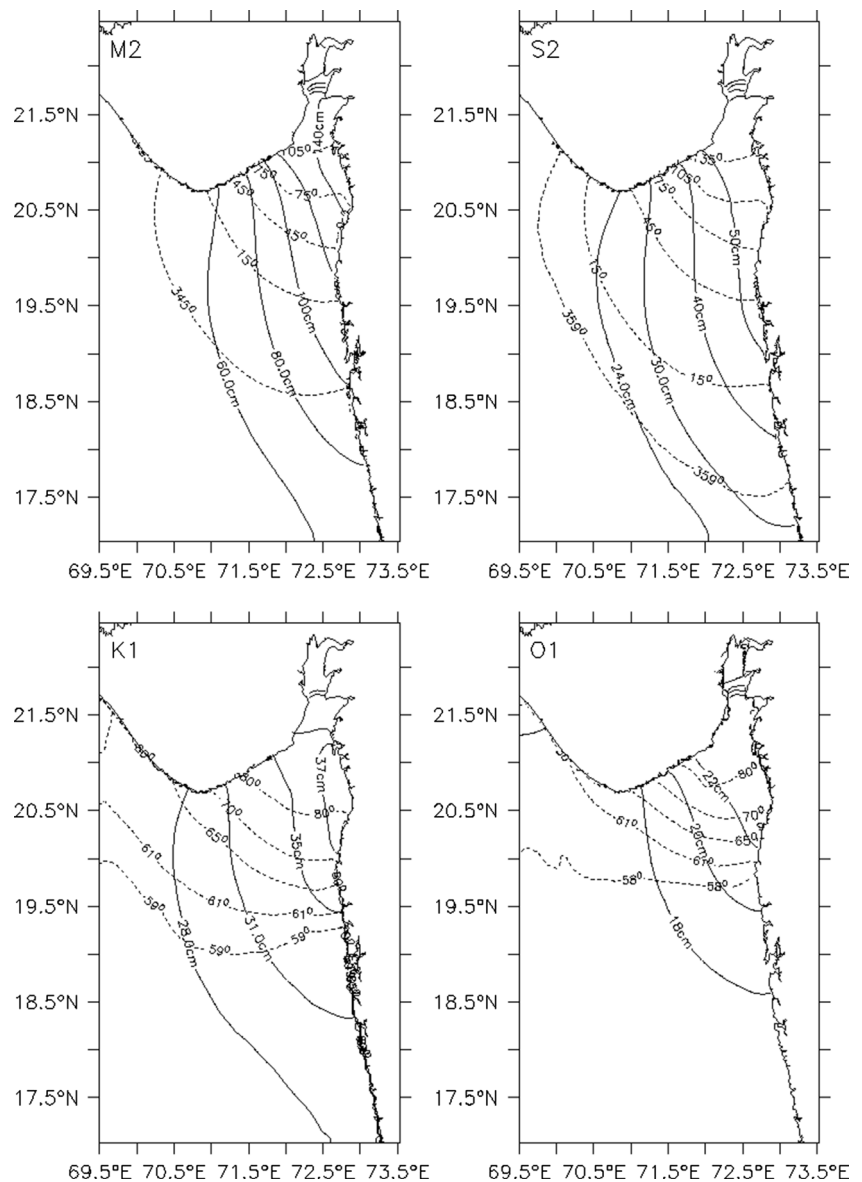
Simulated currents exhibit very pronounce vertical structure. Figure 5 shows the currents along middle of the channel from southwestern corner (Open Ocean regime) to the northeastern corner (inner gulf) at four depths: 10, 30, 80, and 160 m during flood and ebb phases of tides. At the flood phase, surface layer currents over the continental slope are moderate ($<40 \text{ cm s}^{-1}$)

and exhibit anti clock wise rotation with southeast ward flow on the far slope regime and north and north-east ward flow on the near slope regime. At the proximity of the shelf break, currents are weaker southward ($<15 \text{ cm s}^{-1}$). On the shelf, currents are northeastwards and intensified up to 100 cm s^{-1} at middle of the outer gulf. Inside the inner gulf and head regions, currents are southward and very strong (120 cm s^{-1}). Currents at deeper depths follow the similar flow pattern. At the ebb phase, currents (at all depths) mostly prevailed in opposite direction of the flood phase circulation. This result suggests that currents within upper 160 m depths follow barotropic flow pattern. To investigate further the variation of currents on the continental slope regime, vertical slices of the currents and vertical velocity across the slope from far-slope to shelf break are presented in Fig. 6. It shows that currents have more pronounced vertical two-layered structure. During the flood phase, surface layer currents (0–1200 m depth) exhibit anti clockwise rotation with southeastward orientation in the far slope regime and northwestward orientation in the near slope regime. On the other hand, bottom layer currents (below 1200 m depth) exhibit clockwise rotation with northwestward orientation in the far-slope regime and northeast orientation in the near-slope regime. The flow pattern during the ebb phase is opposite to that of the flood phase circulation: clockwise rotation for the surface layer and anti-clockwise rotation for the bottom layer. This slope circulation is associated with strong upwelling and down welling events. Further investigation of slope circulation in the region is beyond the scope of present study.

Residual Circulation

The residual currents determine distribution of various tracers/pollutants etc. in a tidal dominated embayment. The residual circulation resulted from nonlinear interaction between

Fig. 3 Contours of amplitudes (continuous lines) and phases (dash lines) of major tides in the GK and surrounding from the model results



barotropic tides and topography in the study region has been computed from the simulated currents (Methodology), and presented in Fig. 7. The figure also shows the spatial pattern of satellite measured chlorophyll concentration for the month of March based on Sea-Viewing Wide Field-of-View Sensor (SeaWiFS) overlaid with bathymetry. As shown, strong ($>5 \text{ cms}^{-1}$) along channel southward jet circulation prevailed inside the inner gulf. On entering the outer gulf, they intensified on the southeastern flank and then move westward. On the vicinity of the gulf mouth, they parallel the 60 m bathymetry contours and move as isobaths jet currents along northwestward direction. On proceeding, they move as alongshore isobaths coastal jet currents on the northwestern flank of the shelf. These jet currents on the proximity of 60 m depth contour considered as the coastal ocean boundary, which does not allow the gulf-water advected/flushed out into the open

ocean directly. Its consequence can be seen on advection of tracers such as Chlorophyll in this region. These coastal boundary jet currents are associated with an anti-cyclonic (clockwise) eddy on its right side (eastern coastal flank) and cyclonic eddy on its left (western) side. On the proximity of the shelf break, residual currents are mostly southward and strong (5 cms^{-1}) over the shelf (shelf-slope) region and relatively weaker on the slope and open ocean (slope-ocean) regime. This asymmetry in slope circulation is associated with cyclonic eddy on the slope-ocean regime. There are several notable features. Eastward cross-shore currents on reflection near the Mumbai coast bifurcates into northwestward isobaths currents on its northern flank that joins the boundary coastal currents at the gulf mouth and southward propagating alongshore currents on its southern flank that further intensified and propagate as southward alongshore currents.

Fig. 4 Simulated currents and associated tidal levels corresponding to flood and ebb phases: upper panels are for vertical averaged currents and lower panels are for surface currents

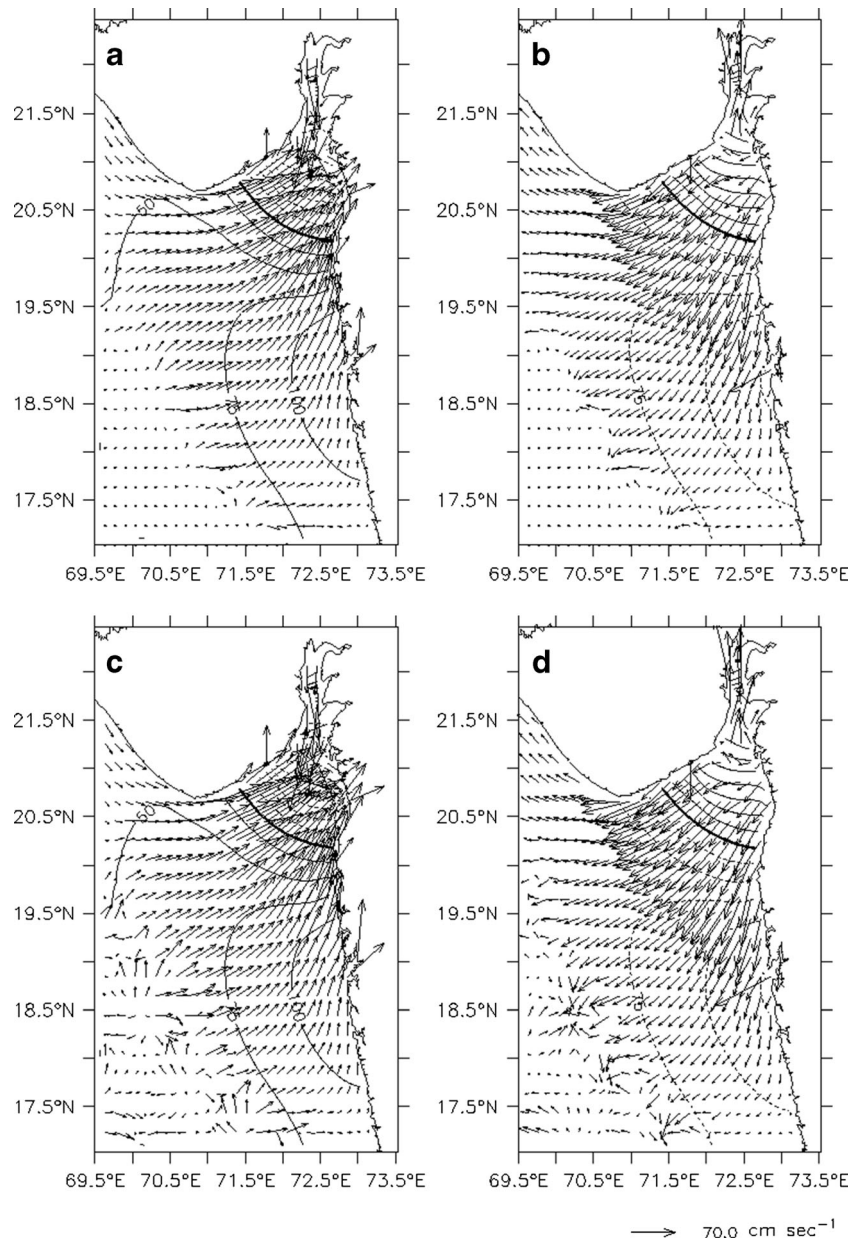


Fig. 5 Simulated flood and ebb phase currents at four depths (10, 30, 80 and 160 m) along the channels of GK and adjacent oceans from south-western corner (far slope regime) to the north-eastern corner (gulf head). Label along X-axis represents indices of the grid numbers along the diagonal of the embayment (see Fig. 1)

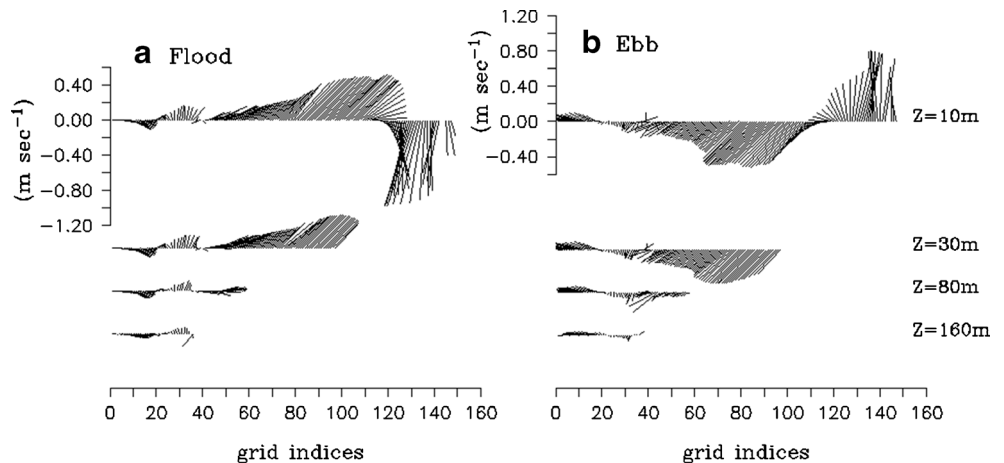
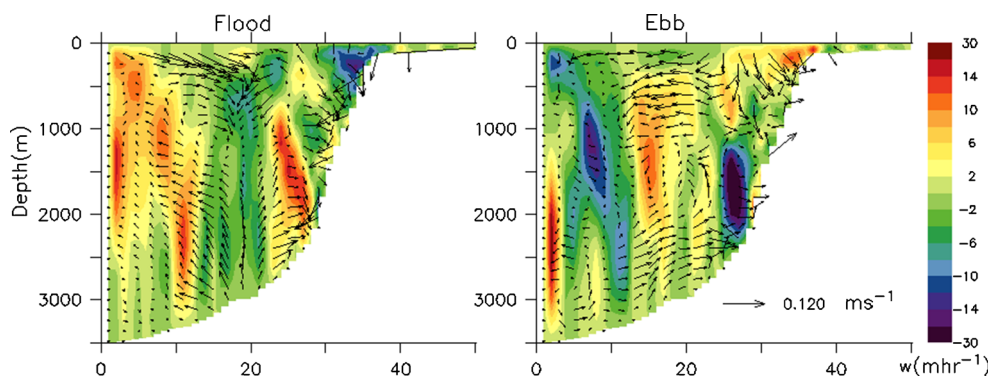


Fig. 6 Vertical structure of simulated horizontal currents and vertical velocity (color) on the continental slope. Label along X-axis represents indices of the grid numbers along the diagonal of the model domain



Most of these features associated with residual currents are seen in the spatial pattern of chlorophyll a concentration (Chla). High intensity Chla advected along the channelling flow inside the inner and outer gulf and elongated westward at the gulf mouth adjacent to the coastal boundary currents. The anti-cyclonic eddy on the northwestern part of the outer gulf is associated with relatively low intensity Chla and the cyclonic eddy on the left (western) side of isobaths coastal boundary

currents, advected the high intensity Chla from the coastal boundary system into the core of the eddy. There exist isolated and relatively intense Chla ($.4 \text{ mg m}^{-3}$) moving along the slope currents. High intensity Chla features ($>1 \text{ mg m}^{-3}$) are observed on the left and right sides of the southward propagating along shore currents on the southeastern flank of the shelf.

Conclusions

We implemented Princeton Ocean Model to study tidal and residual circulation in the Gulf of Khambhat and its adjacent oceans. The model is forced with time varying tidal levels and momentum fluxes at the southern and western boundaries. Simulated tidal levels and circulation pattern in the region compare well the observations. Model currents have pronounced 3D structure, which is matter of further investigation and validation; however, the residual circulations estimated on the region are quite interesting and captured well by the satellite imagery of Chlorophylla concentration on the month of March. This is the period when other forcing such as wind, buoyancy, and freshwater are small and tide dominates the net circulation in the region. This may not be true at all the time, in particular during the monsoonal period. Thus, further investigations, experiments, observation plan and analysis are essential to understand general circulation pattern in the region for different seasons.

Acknowledgments This research work is carried out under a technology development project of National Remote Sensing Centre (NRSC), Hyderabad and Saral ALTIka Science application programme of ISRO-CNES. We thank to our Director for approving the project and providing the necessary support to carry out the work.

References

Admiralty tide tables: Vol. 2. (1996). UK: Hydrographer of the Navy.
 Barltrop, N. D. P. (Editor) (1998). Floating structures: A guide for design and analysis, Volume One, OPL.
 Blumberg, A. F., & Mellor, G. L. (1987). A description of a three-dimensional coastal ocean circulation model. In N. S. Heaps (Ed.),

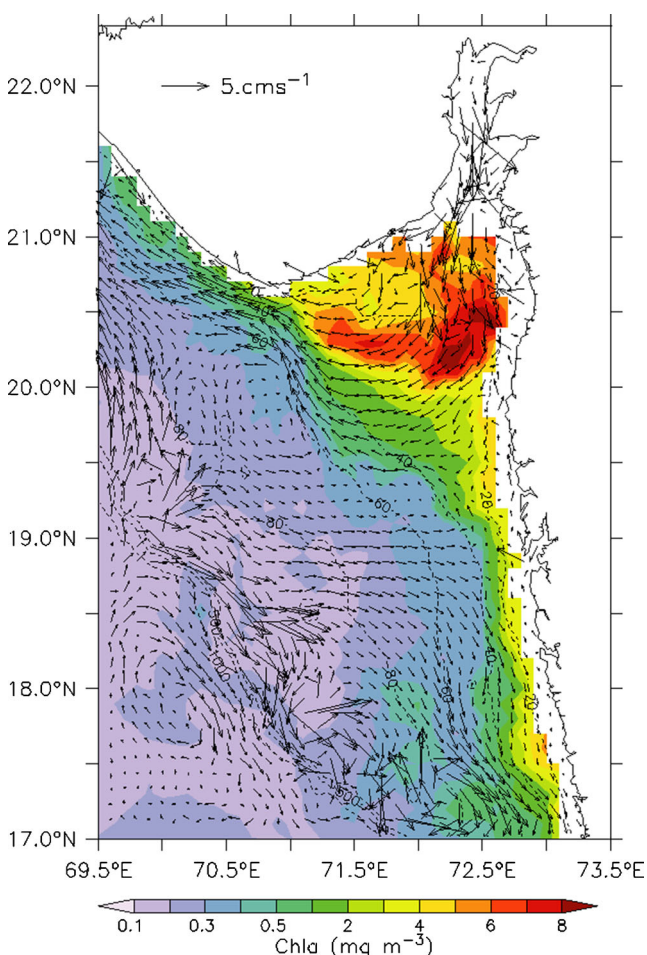


Fig. 7 Residual currents in the GK and adjacent coastal oceans based on simulated currents overlaid with spatial distribution of Chlorophyll (Chla) in March 2003 as measured by SeaWiFS

- Three-dimensional coastal ocean models* (pp. 1–16). Washington, DC: American Geophysical Union.
- Carton, J. A., & Giese, B. S. (2008). A reanalysis of ocean climate using Simple Ocean Data Assimilation (SODA). *Monthly Weather Review*, *136*, 2999–3017.
- Denniss, T., & Middleton, J. H. (1994). Effects of viscosity and bottom friction on recirculating flows. *Journal of Geophysical Research*, *99*(C5), 10,183–10,192. doi:10.1029/93JC03588.
- Foreman, M. G. G. (1978). Manual for tidal currents analysis and prediction. Pacific Marine Science Report 78–6, Institute of Ocean Sciences, Patricia Bay, Victoria, B.C. x. pp.
- Garreau, P., & Mazé, R. (1992). Tidal rectification and mass transport over a shelf break: a barotropic frictionless model. *Journal of Physical Oceanography*, *22*, 719–731.
- Geyer, R. W., & Signell, R. (1990). Measurements of tidal flow around a headland with a shipboard acoustic Doppler current profiler. *Journal of Geophysical Research*, *95*, 3189–3197.
- Hibiya, T. (2004). Internal wave generation by tidal flow over a continental shelf slope. *Journal of Oceanography*, *60*, 637–643.
- Holloway, P. E. (1996). A numerical model of internal tides with application to the AUSTRALIAN northwest shelf. *Journal of Physical Oceanography*, *26*, 21–37.
- Huthnance, J. M. (1986). The Rockall slope current and shelf-edge processes. *Proceedings of the Royal Society of Edinburgh*, *B88*, 83–101.
- International Hydrographic Bureau. (1930). Tides, harmonic constants. Special publication no 26 and addenda. International Hydrographic Bureau.
- Kumar, V. S., & Kumar, K. A. (2010). Waves and currents in tide dominated location off Dahej, Gulf of Khambhat, India, Mar. Geod., vol. 33(2); 218–231.
- Lefèvre, F., Lyard, F., Le Provost, C., & Schrama, E. J. O. (2002). FES99: a tide finite element solution assimilating tide gauge and altimetric information. *Journal of Atmospheric and Oceanic Technology*, *19*(9), 1345–1356.
- Levitus, S. (1982). *Climatological atlas of the world ocean*. Washington D.C: U.S. Government Printing Office. NOAA Professional Paper 13, 173pp.
- Li, S., & McClimans, T. A. (2000). On the stability of barotropic prograde and retrograde jets along a bottom slope. *Journal of Geophysical Research*, *105*(C4), 8847–8855.
- Lyard, F., Lefèvre, F., Letellier, T., & Francis, O. (2006). Modelling the global ocean tides: a modern insight from FES2004. *Ocean Dynamics*, *56*, 394–415.
- Mazé, R., Langlois, G., & Grosjean, F. (1998). Tidal eulerian residual currents over a slope: analytical and numerical frictionless models. *Journal of Physical Oceanography*, *28*, 1321–1332.
- Mellor, G. L., & Yamada, T. (1982). Development of a turbulence closure model for geophysical fluid problems. *Reviews of Geophysics*, *20*, 851–875.
- Nayak, R. K., & Shetye, S. R. (2003). Tides in the Gulf of Khambhat, west coast of India. *Estuarine, Coastal and Shelf Science*, *57*, 249–254.
- Rattray, M., Jr., Dworski, J. G., & Kovala, P. E. (1969). Generation of longinternal waves at a continental slope. *Deep-Sea Research*, *16*(Suppl), 179–195.
- Robertson, R. (2001). Internal tides and baroclinicity in the southern Weddell Sea: Part I: model description, and comparison of model results to observations. *Journal of Geophysical Research*, *106*, 27001–27016.
- Robinson, I. S. (1981). Tidal vorticity and residual circulation. *Deep Sea Research*, *28A*, 195–212.
- Thorpe, S. A. (1992). The generation of internal waves by flow over the rough topography of a continental slope. *Proceedings of the Royal Society of London A*, *439*, 115–130.
- Unnikrishnan, A. S., Shetye, S. R., & Michael, G. S. (1999). Tidal propagation in the Gulf of Khambhat, Bombay High, and surrounding areas. *Proceedings of the Indian Academy of Science (Earth and Planetary Sciences)*, *108*, 155–177.